Quantum Chemistry Investigation of Key Reactions Involved in the Formation of Naphthalene and Indene

S. Fascella, C. Cavallotti,* R. Rota,* and S. Carrà

Politecnico di Milano, Dip. Chimica, Materiali e Ingegneria Chimica "G. Natta"/CIIRCO, Via Mancinelli 7, 20131 Milano, Italy

Received: November 18, 2003; In Final Form: February 12, 2004

Quantum chemistry was used to investigate the kinetics of the reactions of 1,3-C_4H_6 and 1,3-butadien-1-yl with phenyl and benzene, respectively, with the aim of elucidating mechanisms that might lead to the formation of naphthalene and indene. Kinetic constants for each elementary reaction involved in the reactive processes were calculated with density functional theory and a modified G2MP2 method. Small vibrational frequencies, when necessary, were treated as hindered rotors to calculate their rotational potential energies quantum mechanically and the corresponding partition functions. Global rate constants for the formation of the different products were determined with QRRK theory. The main result of this study is that if 1,3-C_4H_6 and 1,3-butadien-1-yl are formed in significant amounts then they can contribute significantly to the formation of naphthalene in a flame. It was also found that activation energies and reaction enthalpy changes can be influenced significantly by the level of theory adopted in the calculations, with B3LYP differing from the more accurate G2MP2 calculations by up to 7 kcal/mol. This was attributed to the known problems of DFT in describing radicals having multiple resonance structures. The calculated rates of formation of indene for the investigated reaction channels were all too slow to compete with alternative mechanisms proposed in the literature.

1. Introduction

Nowadays it is well accepted that air pollution is related to lung cancer and cardiopulmonary disease.[1] At least some of the health hazards of atmospheric pollution can be related to polycyclic aromatic hydrocarbons (PAHs), some of which have been found to be mutagenic,[2] and soot, which represents a major fraction of atmospheric aerosols. Consequently, in the last few years a large amount of attention has been paid to the emissions of PAHs and soot from fossil fuel combustion,[3] which will still represent, at least for the next few decades, the main source of power for humanity.

The minimization of the formation of PAHs and soot in combustion requires the control of chemical processes responsible for their formation and growth. This will be possible only on the basis of a correct physical and chemical understanding of the combustion process. Although many important details about PAHs and soot formation and growth are not yet completely understood, there is general agreement on the main features of the molecular mechanisms involved, as recently reviewed by Ritcher and Howard[4] and summarized in Figure 1. The process starts with the formation of the molecular precursors of soot (that is, heavy PAHs of molecular weight 500−1000 amu) from smaller molecules, followed by the nucleation of heavy PAHs and by the growth of particles either through the successive addition of gaseous molecules or through reactive particle−particle collisions. A slightly different view that was recently proposed suggests that the formation of high-molecular-mass compounds[5] proceeds through the polymerization of small PAHs rather than through the growth of light PAHs by the continuous addition of small molecules.

* To whom correspondence should be addressed. E-mail: carlo.cavallotti@polimi.it. E-mail: renato.rota@polimi.it.

In any case, it is clear that small-PAH formation comes from soot inception and proceeds through reaction paths involving lighter cyclic hydrocarbons. Therefore, kinetic information concerning the formation of small cyclic hydrocarbons (that is, species involving one or two aromatic rings) plays an important role in defining the chemical reaction pathways responsible for PAH and soot formation. In this framework, the importance of fundamental studies aimed at elucidating the relative rates of different reaction channels leading to small PAH is clear. This would in fact allow us to confirm or rule out some reaction patterns.

Following previous work concerning the formation of the first aromatic ring, with particular reference to the competition between six- and five-membered ring species,[6] this work focuses on the formation of the second aromatic ring as a result of the reaction between 1,3-C_4H_6 and 1,3-butadien-1-yl with benzene and phenyl. Being still interested in the rate of production of cyclic species, we paid particular attention to the formation of naphthalene and indene.

In the literature, several tentative formation pathways leading to these species have been proposed, and they have recently been reviewed by Lindstedt et al.[7] Naphthalene can be formed either by HACA-type sequences,[8] which consist of acetylene addition to aromatic radicals followed by a radical abstraction reaction, or by vinylacetylene addition to a phenyl radical,[9] propargyl radical addition to phenyl and methylphenyl radicals,[7] and cyclopentadienyl radicals recombination.[10,11] Indene is supposed to be formed by allene and propargyl radicals' addition to phenyl radicals[12] and acetylene addition to phenyl and methylphenyl radicals.[9]

Unfortunately, despite the extensive work carried out on the identification of the chemical reactions leading to the production of light species with two aromatic rings, there is not yet general

10.1021/jp037518k CCC: $27.50
Published on Web 03/31/2004

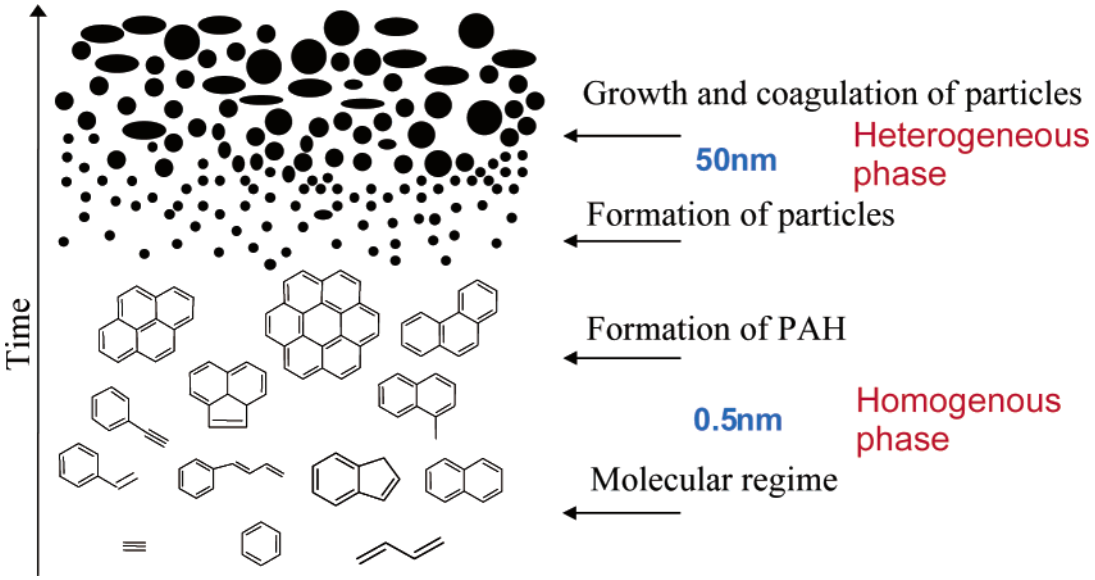

Figure 1. Scheme of soot growth from elementary chemical species (0.5 nm) to large particles (50 nm).[32]

agreement on the dominant formation pathways in a combustion environment.[4] This is true in general and even more for the reaction paths involving C4 species that are often neglected in building detailed kinetic schemes. One of the few exception is represented by a recently proposed pathway leading to naphthalene via the addition of 1,3-butadien-1-yl to benzene.[13]

In this framework, we focused this study on some reactions between C4 species and six-membered ring species leading to the production of naphthalene and indene through cyclization reactions:

$$\left.\begin{matrix} 1,3\text{-}C_4H_6 + C_6H_5 \\ 1,3\text{-}C_4H_5 + C_6H_6 \end{matrix}\right\} \rightarrow C_{10}H_{11}^{l} \rightarrow \begin{cases} C_{10}H_{10}^{C6} + H \rightarrow \text{naphthalene} + H_2 \\ \text{indene} + CH_3 \end{cases}$$

All of the reaction channels investigated in this work involve the formation of a resonantly stabilized radical as a reaction intermediate. Because such radicals are relatively stable as a result of the delocalization of the unpaired electron, they can be formed and react rapidly in the combustion environment.

Because of the lack of experimental information and to allow a fair comparison among different reaction pathways, all of the relevant thermodynamic and kinetic parameters were estimated through quantum chemistry methods. In particular, the geometry of reactants, products, and transition states was optimized by adopting density functional theory (DFT). To investigate the relative importance of the different reaction paths as well as to determine the absolute rate of the overall reactions, we used quantum Rice−Ramsperger−Kassel (QRRK) theory, as modified by Dean[14] to extend it to bimolecular reactions.

Energies were calculated with the G2MP2 theory[6] on geometries optimized at the B3LYP/6-31G(d,p) level. This approach combines the good accuracy of the G2MP2 theory with the lower CPU time requirement of DFT calculations. Moreover, special attention was paid to the investigation of low vibrational frequencies, which are indicative of a small energetic barrier for the relative motion of a part of the molecule with respect to the other. It was found that several internal motions should be treated as hindered rotors. Accordingly, their rotational partition functions were determined, using rotational potentials calculated at the B3LYP/6-31G(d,p) level, through the direct solution of the quantum mechanical equation for a 1D rotor in a potential field. Finally, calculated global kinetic constants were critically compared, whenever possible, with reaction rates of alternative reaction mechanisms proposed in the literature.

2. Method and Theoretical Background

The reactions here investigated are complex processes that involve several elementary reactions. Possible products are naphthalene and indene, generated through a cyclization process, or phenyl butadiene. To describe the overall reacting system, we used quantum Rice−Ramsperger−Kassel (QRRK) theory, as modified by Dean[14] for bimolecular reactions. The extension of QRRK theory to a system containing three excited complexes can be obtained by applying the pseudo-steady stationary approximation (PSSA) to the concentration of every excited complex (denoted in the following text by the * superscript) that is formed as an intermediate step of the global reaction mechanism. With reference to the global scheme and nomenclature reported in Figure 2, it results in the following set of equations:

$$\frac{dC_{10}H_{11}^{C6*}}{dt} = 0 = k_{c6}(E) \cdot C_{10}H_{11}^{l*} - (k_{-C6}(E^{I}) + k_4(E^{I}) + \beta ZM) \cdot C_{10}H_{11}^{c6*} \quad (1)$$

$$\frac{dC_{10}H_{11}^{C5*}}{dt} = 0 = k_{c5}(E) \cdot C_{10}H_{11}^{l*} - (k_{-C5}(E^{II}) + k_2(E^{II}) + \beta ZM) \cdot C_{10}H_{11}^{c5*} \quad (2)$$

$$\frac{dC_{10}H_{11}^{l*}}{dt} = 0 = k_1(E) \cdot C_6H_5 \cdot C_4H_6 - (k_{-1}(E) + k_3(E) + k_{c6}(E) + k_{c5}(E) + \beta ZM) \cdot C_{10}H_{11}^{l*} + k_{-c6}(E^{I}) \cdot C_{10}H_{11}^{c6*} + k_{-c5}(E^{II}) \cdot C_{10}H_{11}^{c5*} \quad (3)$$

where k_i are the kinetic constants of the elementary reactions and βZM is the rate of the collisional stabilization reaction. Z is the collisional frequency calculated through the kinetic theory of gases, M is the concentration of the bath gas, and β is the efficiency factor for the transmission of energy that was calculated as suggested by Troe[15] using the mean energy

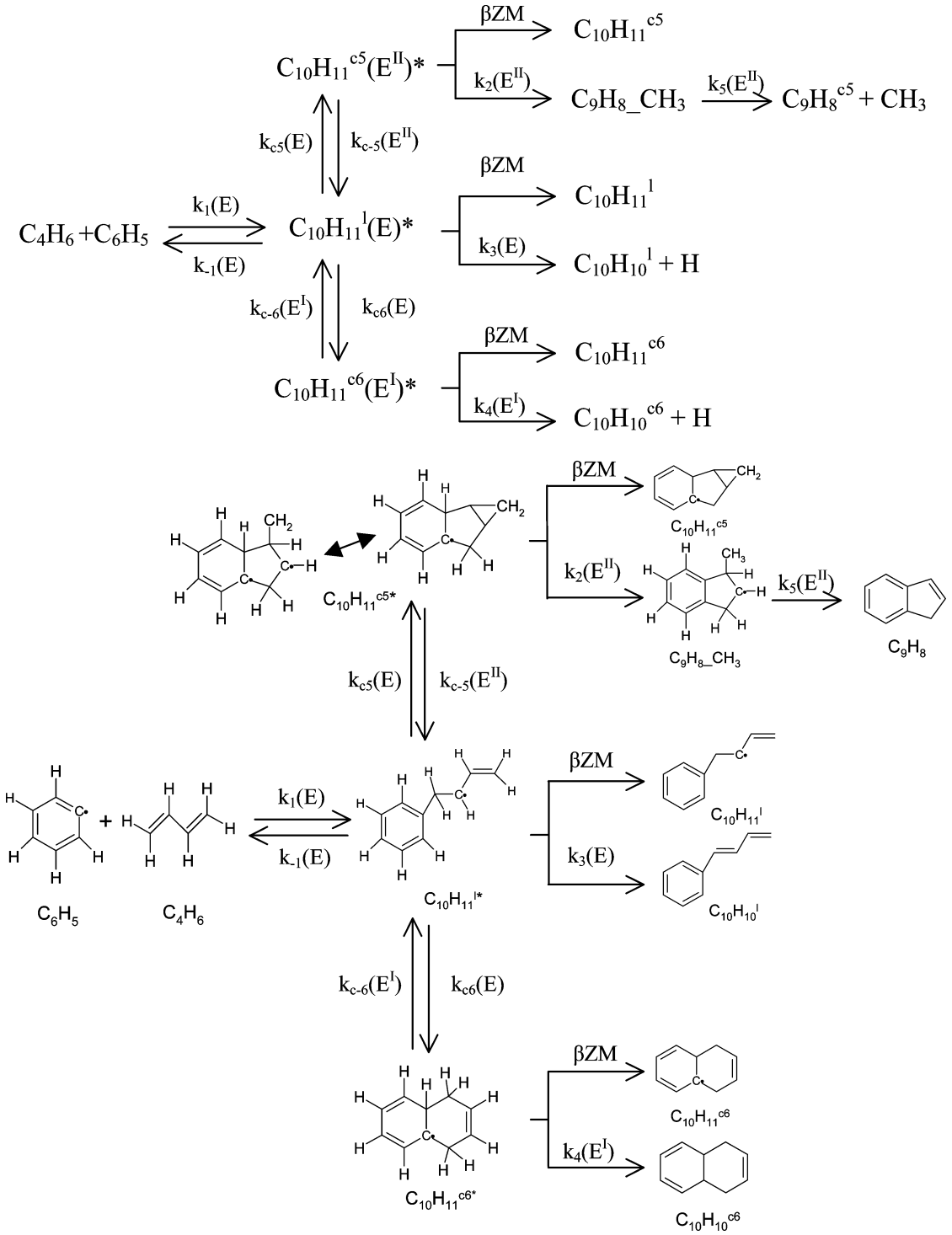

Figure 2. Kinetic pathway following the reaction of the addition of 1,3-C_4H_6 to C_6H_5.

transferred per collision of 980 cal/mol. This is consistent with considering N_2 to be a collision partner, which is a reasonable assumption because it is the most abundant species in a fuel−air combustion environment. The kinetic constant of each reaction i involving the kth excited complex, $C_{10}H_{11}^{k*}$, can be calculated from QRRK theory as

$$k_i^{rxn} = \sum_{E=E_{crit}}^{\infty} k_i(E) \cdot C_{10}H_{11}^{k*} \cdot f(E) \qquad (4)$$

where E_{crit} is the activation energy for the considered reaction, measured from the bottom of the potential energy well for each excited species, and $f(E)$ is the chemical activation distribution function. The energies of the excited complexes E, E^I, and E^{II} for $C_{10}H_{11}^{l*}$, $C_{10}H_{11}^{c6*}$, and $C_{10}H_{11}^{c5*}$, respectively (see Figure 2), are related to each other by the enthalpy changes of the cyclization reactions as $E^I = E - \Delta H^{c6}$ and $E^{II} = E - \Delta H^{c5}$. The parameters required by QRRK are the rate of intermolecular energy transfer between excited and nonexcited species, the kinetic constants (preexponential factor and activation energy) for each elementary reaction, and the mean vibrational frequencies for every chemical species involved in the global kinetic scheme. Few of these parameters are known experimentally and were thus calculated using ab initio methods. For each elemen-

tary reaction, forward kinetic constants were evaluated with quantum chemistry and transition-state theory, and backward kinetic constants were determined by applying thermodynamic consistency (i.e., from the equilibrium constant) with calculated enthalpy and entropy changes. All calculations were performed using the Gaussian 98 suite of programs[16] at different levels of theory. Geometries were optimized using density functional theory (DFT), with exchange and correlation energies calculated with Becke's three parameters and the Lee−Yang−Parr functionals (B3LYP)[17] using the 6-31G(d,p) basis set. Frequency calculations were performed at the same level of theory both to calculate the vibrational frequencies of each adduct, required as input to QRRK, and to verify the stability of reactants, products, and transition states. In particular, calculated transition-state (TS) structures were characterized by the presence of a single imaginary frequency, and stable chemical species were characterized by the absence of imaginary frequencies. Successively, to improve the level of description of the system, the energy of every molecule was calculated using an approach similar to G2MP2, to which we refer in the following text as G2MP2*.[18] G2MP2 theory is based on a combination of perturbation and configuration interaction methods, and it was developed with the goal of evaluating bond energies, heats of formation, and electron affinities of atoms and molecules with chemical accuracy (i.e., within 1−2 kcal/mol from the experimental value).[19] The energy of the molecule is first calculated at the QCISD(T)/6-311+G(d,p) level and corrected for basis set error by subtracting the energy calculated at the MP2/6-311+G(d,p) level from that calculated at the MP2/6-311+G(3df,2p) level. The difference between G2MP2 and G2MP2* is that G2MP2 structures are calculated at the MP2/6-31G(d,p) level and vibrational frequencies are calculated at the HF/6-31G(d,p) level, whereas in G2MP2* we optimized structures and calculated vibrational frequencies at the B3LYP/6-31G(d,p) level, which for the type of molecules here considered should be more accurate. G2MP2* increases the accuracy of the calculated energies with respect to DFT at the expanse of a significant increase in computational time. Summarizing, the molecular energy was calculated as

$$E = E(\text{QCISD(T)/6-311+g(d,p)}) + E(\text{MP2/6-311+g(3df,2p)}) - E(\text{MP2/6-311+g(d,p)}) + \text{ZPE} + \text{T.E.} + \text{HLC} \quad (5)$$

where HLC is the higher-level correction term proposed for the original G2MP2 theory.[18] Kinetic constants of elementary reactions were calculated using conventional transition-state theory[20] as

$$k = \frac{k_B \cdot T}{h} \cdot \frac{Q^{\neq}}{Q^R} \cdot k^{\neq} \quad (6)$$

where k_B is the Boltzman constant, h is the Planck constant, T is the reference temperature (300 K), Q represents the products of the partition functions of transition states ($\neq$) and reactants (R), and $k^{\neq}$ is the Wigner correction for tunneling.[21]

Particular attention was paid to the calculation of vibrational frequencies. In fact, a low vibrational frequency is indicative of a small energy barrier for the relative motion of a part of the molecule with respect to the other one. Because every internal rotation in a molecule occurs in the presence of a potential energy barrier, we analyzed the possibility that low vibrational frequencies might degenerate in torsional rotors or bendings. This analysis was carried out for reactants, products, and transition states with quantum chemistry. Thus, as a general rule, we calculated the potential energy as a function of the rotational angle for internal motions corresponding to vibrational frequencies smaller than 150 cm^{-1} at the B3LYP/6-31G(d,p) level, and the calculated potential energy was interpolated using cubic splines. As suggested by Van Speybroeck et al.,[22] we used the calculated potential energy, $V(\phi)$, to solve the rotational 1D Schrödinger equation:

$$-\frac{\hbar^2}{2I_m}\frac{\partial^2\Psi}{\partial\phi^2} + V(\phi)\cdot\Psi(\phi) = \epsilon\cdot\Psi(\phi) \quad (7)$$

where $\hbar$ is the ratio between the Planck constant and 2π and I_m is the reduced moment of inertia of a part of the molecule with respect to the other one calculated either as[23]

$$I_m = I_a\left(1 - \sum_{i=X,Y,Z}\frac{I_a\lambda_{mi}^2}{I_i}\right) \quad (8)$$

where I_a is the moment of inertia of the mth top and λ_{mi} is the direction cosine between the axis of the mth top and the principal axis of the whole molecule, or as[24]

$$I_m = \frac{I_1\cdot I_2}{I_1 + I_2} \quad (9)$$

where I_1 and I_2 are the moments of inertia of the two rotating moieties. Equation 9 was used when the two rotating parts of the molecule had similar moments of inertia, and eq 8 was used in the other cases. In eq 7, ϵ represents the energy levels associated with each vibrational frequency, and ϕ is the rotational angle. The Schrödinger equation (eq 7) was numerically solved using the finite difference method for ϕ values between 0 and 2π. At each calculated eigenvalue ϵ_k, there is a corresponding accessible rotational energy level. The internal rotation partition function was then calculated as

$$q_{\text{rot,int}} = \frac{1}{\sigma_{\text{int}}}\sum_k g_k\cdot\exp\left(-\frac{\epsilon_k}{k_B T}\right) \quad (10)$$

where g_k is the degeneracy of rotational energy level ϵ_k and σ_{int} is the symmetry number of the internal rotation.

3. Results and Discussion

3.1. Activation Energies and Enthalpy Changes for 1,3-C_4H_6 + C_6H_5. The global scheme for the reaction of the addition of 1,3-C_4H_6 to C_6H_5 is shown in Figure 2. 1,3-C_4H_6 and C_6H_5 first react to form the linear decadienyl radical $C_{10}H_{11}^{l}$. Because this reaction is exothermic, the adduct is in a vibrationally excited state ($C_{10}H_{11}^{l*}$). Then $C_{10}H_{11}^{l*}$ can follow five different reaction pathways. It can either lose its excitation energy by collision with the bath gas to give nonexcited $C_{10}H_{11}^{l}$. Alternatively, it can cyclize to form the cyclopentadienyl radical ($C_{10}H_{11}^{c5*}$) or the cyclohexenyl radical ($C_{10}H_{11}^{c6*}$). Finally, it can dissociate into the reactants to give back 1,3-C_4H_6 and C_6H_5 or lose a hydrogen atom, forming $C_{10}H_{10}^{l}$. Both the $C_{10}H_{11}^{c5*}$ and $C_{10}H_{11}^{c6*}$ adducts are in an excited state due to the exothermicity of their formation reactions, with an excitation energy equal to that of $C_{10}H_{11}^{l*}$, from which they are produced, plus the reaction-energy change. Their reactivity is similar to that of $C_{10}H_{11}^{l*}$. They can either collide with the bath gas to give the nonexcited $C_{10}H_{11}^{c5}$ and $C_{10}H_{11}^{c6}$ species or open the ring to give back $C_{10}H_{11}^{l*}$ or dissociate. In particular, $C_{10}H_{11}^{c6*}$ can

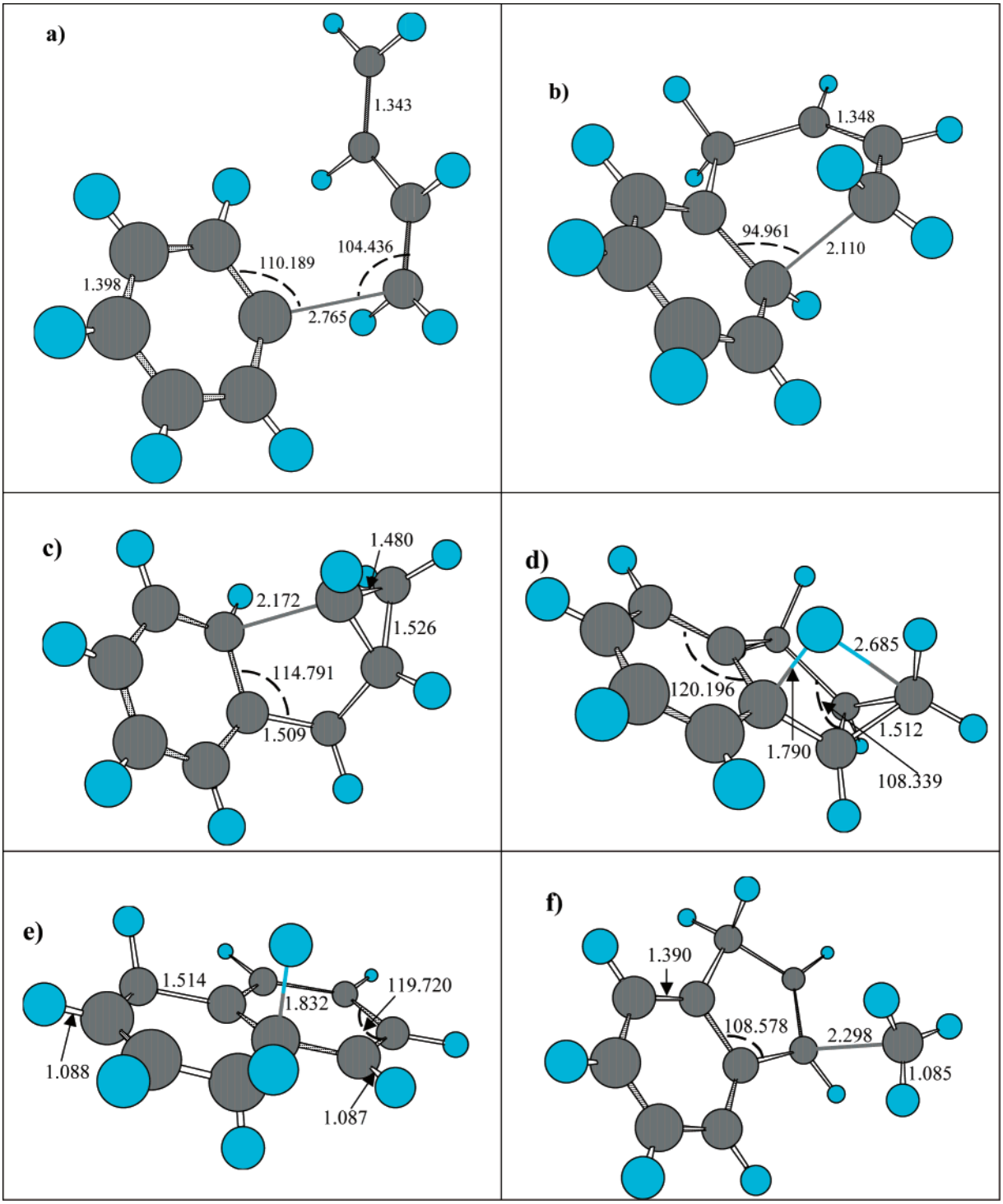

Figure 3. Transition-state structures for reactions (a) 1,3-C_4H_6 + C_6H_5 → $C_{10}H_{11}^{l}$, (b) $C_{10}H_{11}^{l}$ → $C_{10}H_{11}^{c6}$, (c) $C_{10}H_{11}^{l}$ → $C_{10}H_{11}^{c5}$, (d) $C_{10}H_{11}^{c5}$ → C_9H_8_CH_3, (e) $C_{10}H_{11}^{c6}$ → $C_{10}H_{10}^{c6}$ + H, and (f) C_9H_8_CH_3 → $C_9H_8^{c5}$ + CH_3. Distances are reported in angstroms, and angles are reported in degrees.

dissociate directly to give $C_{10}H_{10}^{c6}$ and H, whereas the dissociation of $C_{10}H_{11}^{c5}$ involves at first the formation of the methylcyclopentenyl (C_9H_8_CH_3) radical followed by the loss of methyl to form indene ($C_9H_8^{c5}$). Transition-state structures calculated at the B3LYP/6-31G(d,p) level for some key reactions of this kinetic scheme are shown in Figure 3, where some important geometrical parameters of these structures are also reported.

Enthalpy changes calculated at different levels of theory are reported in Table 1. It can be observed that the computed reaction enthalpies can differ significantly depending on the level of theory used. In this framework, G2MP2* calculations can be considered to be the most accurate of those here performed, as discussed elsewhere.[6] However, it is also known that calculations performed at the B3LYP/6-31G(d,p) level are often in good agreement with experimental data.[4] Thus, the relatively large differences between values calculated for some reactions at the B3LYP/6-31G(d,p) and G2MP2* levels and reported in Table 1 were unexpected and deserve some discussion. First, it must be pointed out that the overall qualitative reaction trends predicted by the two methods are the same. For instance, the formation of the 1,4,9-trihydronaphthyl radical ($C_{10}H_{11}^{c6}$) is

TABLE 1: Comparison between Reaction Enthalpy Changes (kcal/mol) Calculated at 298 K and 1 atm with Different Quantum Chemistry Theories[a]

	B3LYP 6-31 g(d,p)	QCISD(T) 6-311+g(d,p)	MP2 6-311+g(3df,2p)	MP2 6-311+g(d,p)	G2MP2*
$1,3\text{-}C_4H_6 + C_6H_5 \rightarrow C_{10}H_{11}^{l}$	−45.8	−50.8	−71.5	−71.0	−49.4
$C_{10}H_{11}^{l} \rightarrow C_{10}H_{11}^{c5}$	23.8	16.3	26.7	25.3	18.1
$C_{10}H_{11}^{l} \rightarrow C_{10}H_{11}^{c6}$	8.03	1.1	13.9	12.8	2.9
$C_{10}H_{11}^{c5} \rightarrow C_9H_8^{c5} + CH_3$	−8.9	−0.6	−19.2	−17.6	−5.6
$C_{10}H_{11}^{l} \rightarrow C_{10}H_{10}^{l} + H$	43.2	45.3	34.3	35.6	39.2
$C_{10}H_{11}^{c6} \rightarrow C_{10}H_{10}^{c6} + H$	22.8	26.8	2.0	3.7	20.5
$1,3\text{-}C_4H_6 + C_6H_5 \rightarrow C_9H_8^{c5} + CH_3$	−30.9	−35.1	−64.0	−63.3	−36.9
$1,3\text{-}C_4H_6 + C_6H_5 \rightarrow C_{10}H_{10}^{c6} + H$	−14.97	−22.9	−55.6	−54.5	−26.0
$1,3\text{-}C_4H_6 + C_6H_5 \rightarrow C_{10}H_{10}^{l} + H$	−2.6	−5.5	−37.2	−35.4	−10.2

[a] G2MP2* differs from G2MP2 in that geometries were optimized at the B3LYP/6-31 g(d,p) level. All energies are corrected for ZPE and thermal energies with frequencies calculated at the B3LYP/6−31 g(d,p) level.

TABLE 2: Calculated Activation Energies (kcal/mol) for Forward and Backward Reactions[a]

	reaction	$E_{a,forw}$	$E_{a,back}$
k_1	$1,3\text{-}C_4H_6 + C_6H_5 \rightarrow C_{10}H_{11}^{l}$	0.	48.9
k_{c5}	$C_{10}H_{11}^{l} \rightarrow C_{10}H_{11}^{c5}$	45.0	25.9
k_{c6}	$C_{10}H_{11}^{l} \rightarrow C_{10}H_{11}^{c6}$	24.5	20.7
k_2	$C_{10}H_{11}^{c5} \rightarrow C_9H_8^{c5}\_CH_3$	24.9	51.7
k_3	$C_{10}H_{11}^{l} \rightarrow C_{10}H_{10}^{l} + H$	46.8	8.8
k_4	$C_{10}H_{11}^{c6} \rightarrow C_{10}H_{10}^{c6} + H$	31.9	8.9
k_5	$C_9H_8^{c5}\_CH_3 \rightarrow C_9H_8^{c5} + CH_3$	31.5	12.1

[a] Geometries were optimized with B3LYP/6-31g(d,p), frequencies calculated with B3LYP/6-31g(d,p), and energies were calculated with G2MP2*.

predicted to be more favored than that of the 3-methyl indenyl radical ($C_{10}H_{11}^{c5}$) both by DFT calculations (8.03 vs 23.8 kcal/mol) and G2MP2* (2.9 vs 18.1 kcal/mol). Similarly, for both DFT and G2MP2* calculations, among the possible products of the addiction reaction of $1,3\text{-}C_4H_6$ to C_6H_5, namely, $C_9H_8^{c5}$, $C_{10}H_{10}^{c6}$, and $C_{10}H_{10}^{l}$, the most exothermic reaction pathway is that leading to the formation of $C_9H_8^{c5}$. The different results in terms of absolute values of the two calculation methods can probably be ascribed to well-known difficulties of DFT in treating molecules with different resonance structures.[25,26]

It is also interesting to compare the reaction enthalpies calculated at the G2MP2* level with those determined in our previous work for the reaction between $1,3\text{-}C_4H_6$ and C_2H_3.[6] This reaction is similar to the one here investigated in that it involves the formation of the first aromatic ring, whereas in the present work we have investigated the formation of the second aromatic ring through the addition of the same reactant (namely $1,3\text{-}C_4H_6$) to C_6H_5. In particular, we found that the reaction $C_6H_5 + 1,3\text{-}C_4H_6 \rightarrow C_{10}H_{11}^{l}$ is exothermic by 49.4 kcal/mol; that is, it is 4.3 kcal/mol higher than the enthalpy change calculated for the $C_2H_3 + 1,3\text{-}C_4H_6 \rightarrow C_6H_9^{l}$ reaction. The higher energy of the $C_4H_6-C_6H_5$ bond with respect to the $C_4H_6-C_2H_3$ bond can be explained in terms of an effect of hyperconjugation of the phenyl aromatic ring with butadiene, as proposed by Carrà et al.[27] The activation energies for the dissociation of $C_2H_3\_C_4H_6$ and $C_6H_5\_C_4H_6$ are similar (48.9 vs 48.7), which we ascribed to the fact that the hyperconjugation effect decreases significantly as the distance between the two separating moieties increases. Calculated activation energies (at the G2MP2* level) for the considered reactions are reported in Table 2. It can be observed that the activation energy for the formation of $C_{10}H_{11}^{l*}$ is zero, whereas the backward reaction

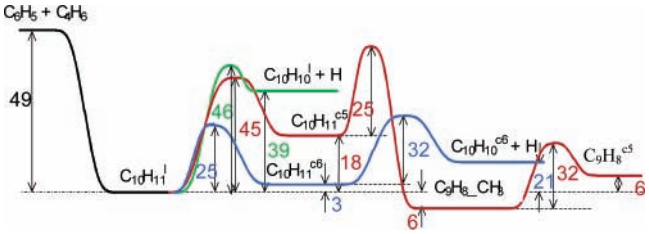

Figure 4. Enthalpy changes and activation energies for the kinetic pathway following the reaction of the addition of $1,3\text{-}C_4H_6$ to C_6H_5 (kcal/mol). Values were calculated with the G2MP2* theory.

has an activation energy equal to 48.9 kcal/mol, which implies that $C_{10}H_{11}^{l*}$ dissociation into the reactants is a slow process. Moreover, once $C_9H_8\_CH_3$ is produced, it is more likely to dissociate into $C_9H_8^{c5}$ and CH_3 rather than give back $C_{10}H_{11}^{c5*}$ because the activation energy necessary to form $C_9H_8\_CH_3$ from $C_{10}H_{11}^{c5*}$ is much higher than that required to decompose into $C_9H_8^{c5}$ and CH_3 (51.7 vs 31.5 kcal/mol). Therefore, in all of the following calculations, we assumed that the reactions leading from $C_{10}H_{11}^{c5*}$ to $C_9H_8{}^{c5}$ can be summarized in a single reaction step with an overall rate equal to that of the conversion of $C_{10}H_{11}^{c5*}$ to $C_9H_8\_CH_3$. Activation energies and enthalpy changes calculated for the investigated reaction scheme are reported schematically in Figure 4.

3.2. Treatment of Low Vibrational Frequencies. As previously mentioned, dedicated work has been carried out to analyze the structural dynamics of a few molecules and transition states possessing low vibrational frequencies. The investigated molecules were the transition state for the reaction of the addition of $1,3\text{-}C_4H_6$ to C_6H_5, the transition state for the dissociation reaction of $C_9H_8\_CH_3$, the transition state for the dissociation reaction of $C_{10}H_{11}^{l*}$ to $C_{10}H_{10}{}^{l}$ and H, and the $C_{10}H_{11}^{l}$ molecule.

The transition state of the reaction between $1,3\text{-}C_4H_6$ and C_6H_5 presents five low vibrational frequencies, namely, 22.4, 34.8, 40.2, 82.3, and 120.1 cm^{-1}. For each frequency, an analysis of the potential energy corresponding to the internal rotation was performed. It was found that the 22.4-cm^{-1} frequency corresponds to the torsional motion around the $C_4H_6-C_6H_5$ bond. Because the maximum of the energy barrier of this internal rotation is very low (about 0.6 kcal/mol), as shown in Figure 5a, it was considered to be a hindered internal rotor. The associated partition function significantly changes when calculating it as a rotor (26.5) rather than as a vibration (9.81). The two higher frequencies (i.e., 82.3 and 120.1 cm^{-1}) show a similar behavior. They can be attributed to the rocking motion

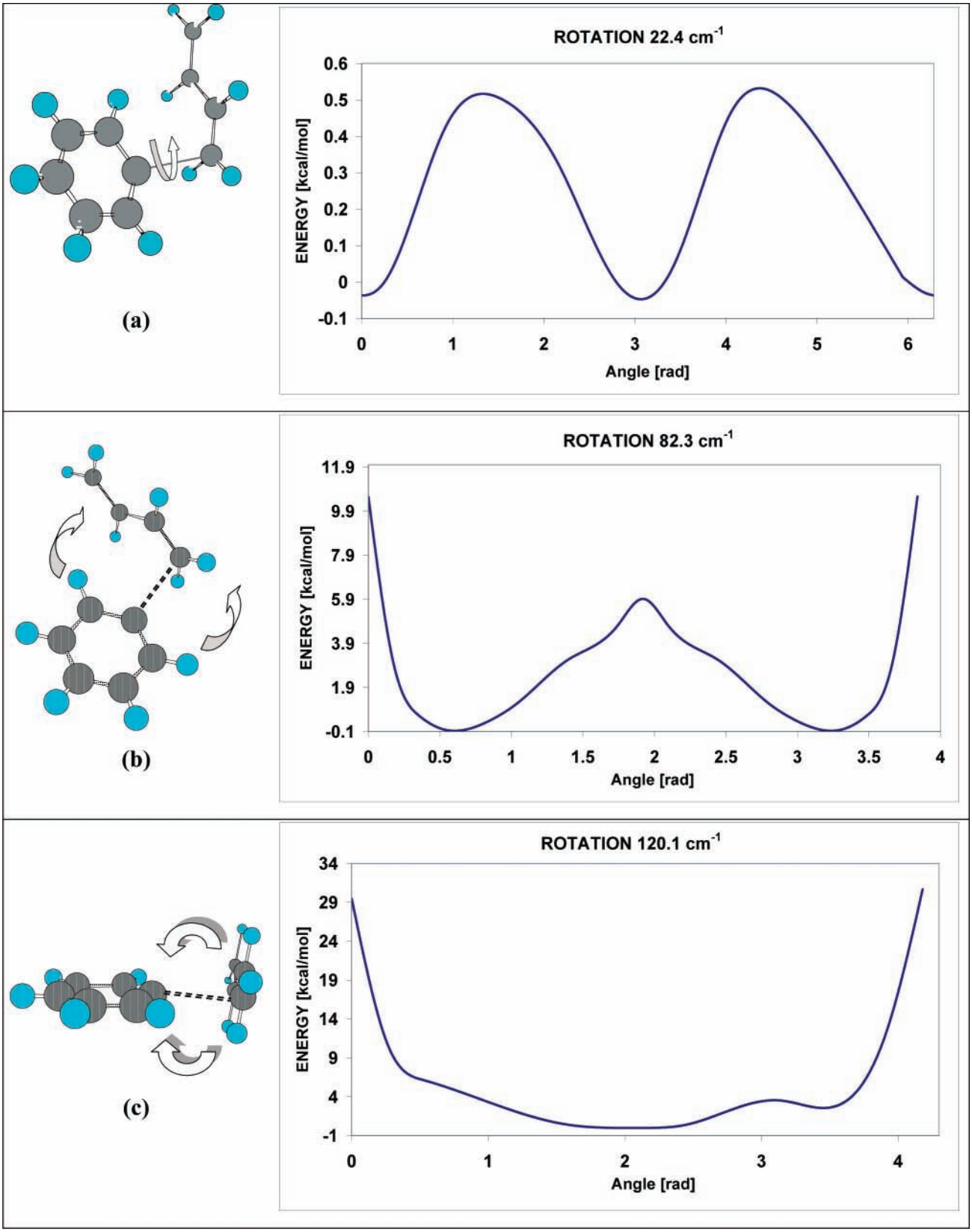

Figure 5. Rotational potential energy for the internal bendings of the transition state for the reaction 1,3-C_4H_6 + C_6H_5 → $C_{10}H_{11}^{l}$.

of the C_4H_6 fragment with respect to the $C_4H_6-C_6H_5$ bond. The analysis of the rotational potential energy has shown that these rotations are significantly hindered so that the rotational domain is smaller than 360°. The calculated values were 220° for the first bending and 240° for the second one. The related energy barriers are shown in Figure 5b and c. The corresponding rotational partition functions calculated through the solution of eq 7 are equal to 17.46 and 13.44, which are again significantly different from the values of their vibrational partition functions (3.06 and 2.28, respectively). Finally, the 34.8- and 40.1-cm^{-1} vibrational frequencies can be attributed to the rocking motion of the C_6H_5 fragment with respect to the $C_4H_6-C_6H_5$ bond.

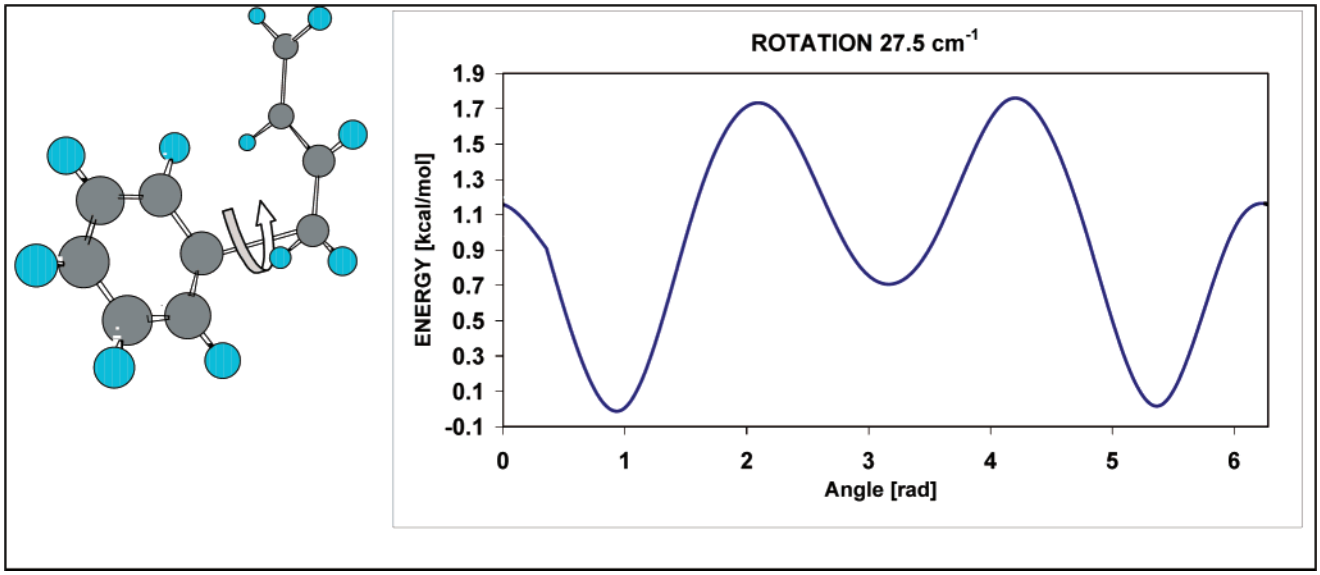

Figure 6. Rotational potential energy for one of the two active internal rotations of $C_{10}H_{11}^{l}$.

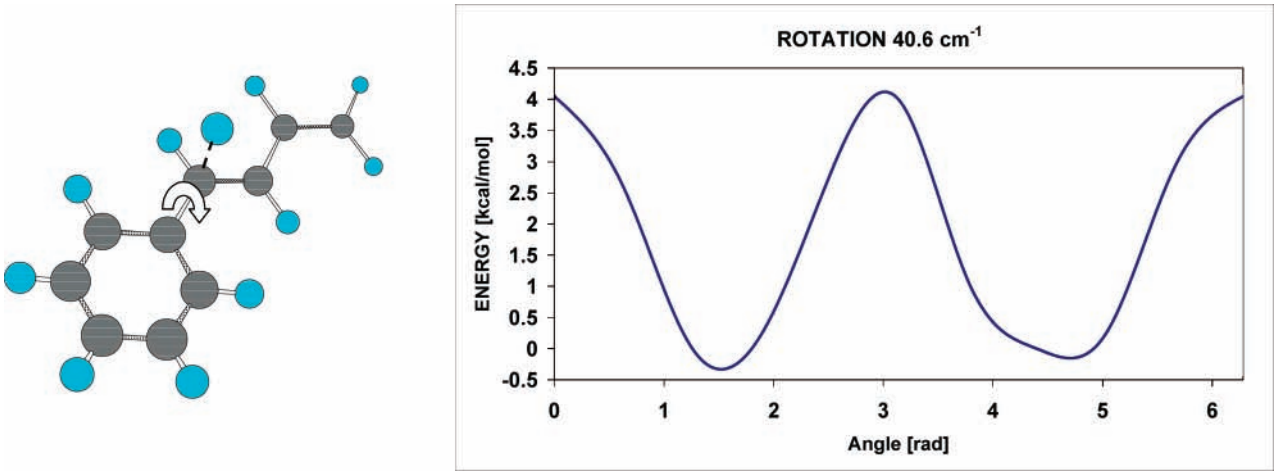

Figure 7. Rotational potential energy for the active internal rotations of the transition state for the $C_{10}H_{11}^{l} \rightarrow C_{10}H_{10} + H$ reaction.

Because of the very high energy barriers calculated when studying the internal motions corresponding to these vibrational frequencies, we concluded that they can be considered to be vibrations.

The same analysis was carried out for the $C_{10}H_{11}^{l*}$ adduct. In Figure 6 is reported, together with the computed energy barrier, one of the two internal motions of the C_4H_6 fragment that were treated as hindered rotors. The rotation corresponds to the motion of C_6H_5 and C_4H_6 around the butadiene−phenyl bond. A comparison with the same motion in the transition state of the 1,3-$C_4H_6 + C_6H_5 \rightarrow C_{10}H_{11}^{l}$ reaction shows that the maximum of the energy barrier is larger (1.9 vs 0.6 kcal/mol), probably because of increased steric hindrance. (See Figure 6.) The second motion corresponds to the rotation of the propargyle group in the butadienic tail. Also, in this case, the hindered rotational partition functions (11.90 and 13.35) are higher than the vibrational ones (8.62 and 4.61). Another small vibrational frequency that was treated as a torsional rotor was the rotation of the methyl group in the transition state of the $C_9H_8\_CH_3 \rightarrow C_9H_8^{c5} + CH_3$ reaction, whose partition function triples its value on passing from vibrational (2.57) to rotational (8.95).

Finally, the internal motion of the butadienic tail in the transition state of the $C_{10}H_{11}^{l} \rightarrow C_{10}H_{10}^{l} + H$ reaction was analyzed. The calculated rotational potential energy is shown in Figure 7. Also, in this case, the motion can be treated as a hindered rotation, resulting in a partition function equal to 8.95 (vs 2.57 if calculated as a vibration). The comparison between vibrational and rotational partition functions for the structures here studied is summarized in Table 3.

TABLE 3: Comparison between Vibrational (Q_{vib}) and Internal Rotational (Hindered and Free) Partition Functions for Significant Low Vibrational Frequencies[a]

	υ [cm^{-1}]	Q_{vib}	Q_{rot}^{hind}	Q_{rot}^{free}
TST1 internal rotor (Figure 5a)	22.4	9.81	26.51	38.24
TST1 1° bending (Figure 5b)	82.3	3.06	17.46	66.02
TST1 2° bending (Figure 5c)	120.1	2.28	13.44	62.78
$C_{10}H_{11}^{l}$ butadiene rotation (Figure 6)	25.7	8.62	11.90	38.75
$C_{10}H_{11}^{l}$ propargyle rotation	51	4.61	13.35	30.91
TST2 methyl rotation	102.7	2.57	8.95	9.77
TST3 butadiene rotation (Figure 7)	40.6	5.65	14.75	39.43

[a] TST1, TST2, and TST3 are the transition-state structures for 1,3-$C_4H_6 + C_6H_5 \rightarrow C_{10}H_{11}^{l}$, $C_9H_8\_CH_3 \rightarrow C_9H_8^{c5} + CH_3$, and $C_{10}H_{11}^{c6} \rightarrow C_{10}H_{10}^{c6} + H$ reactions, respectively.

Using these values, preexponential factors of the investigated reactions were calculated through conventional transition-state theory and are reported in Table 4. The importance of the aforementioned treatment of low frequencies should be stressed.

TABLE 4: Calculated TST Kinetic Constants ($k = A \cdot T^{\alpha} \cdot \exp(-E/RT)$)[a]

	reaction	A_{forw}	α	$E_{a,forw}$	A_{back}	α	$E_{a,back}$
k_1	$1,3\text{-}C_4H_6 + C_6H_5 \rightarrow C_{10}H_{11}^{l}$	1.5×10^{12}	0.	0.	8.3×10^{17}	−1.	48.9
k_{c5}	$C_{10}H_{11}^{l} \rightarrow C_{10}H_{11}^{c5}$	3.1×10^{10}	0.	45.0	1.5×10^{12}	0.	25.9
k_{c6}	$C_{10}H_{11}^{l} \rightarrow C_{10}H_{11}^{c6}$	4.6×10^{10}	0.	24.5	1.7×10^{12}	0.	20.7
k_2	$C_{10}H_{11}^{c5} \rightarrow C_9H_8\_CH_3$	4.0×10^{12}	0.	24.9	1.6×10^{12}	0.	51.7
k_3	$C_{10}H_{11}^{l} \rightarrow C_{10}H_{10}^{l} + H$	2.4×10^{12}	0.	46.8	5.2×10^{12}	0.	8.8
k_4	$C_{10}H_{11}^{c6} \rightarrow C_{10}H_{10}^{c6} + H$	7.8×10^{12}	0.	31.9	3.5×10^{12}	0.	8.9
k_5	$C_9H_8\_CH_3 \rightarrow C_9H_8^{c5} + CH_3$	5.0×10^{13}	0.	31.5	2.0×10^{11}	0.	12.1

[a] Kinetic parameters are reported in units consistent with kcal, s, mol, and cm and were determined by treating low vibrational frequencies as internal rotors, when necessary. The rate coefficients of the backward reactions were evaluated through thermodynamic consistence with calculated free-energy changes.

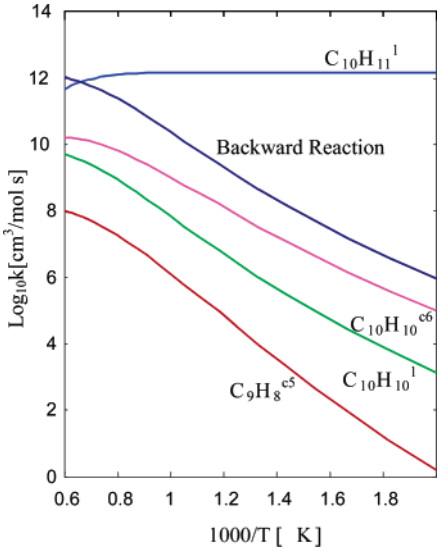

Figure 8. QRRK rate constants calculated for the addition of C_6H_5 to $1,3\text{-}C_4H_6$ at 1 atm. All possible products were considered. Backward reaction refers to $C_{10}H_{11}^{l*} \rightarrow C_6H_5 + 1,3\text{-}C_4H_6$.

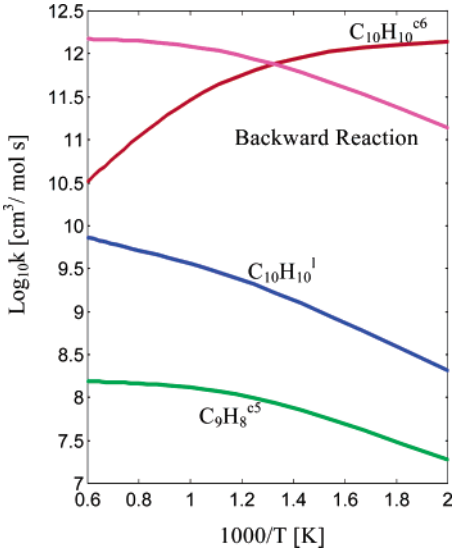

Figure 9. QRRK rate constants calculated for the reaction of C_6H_5 with $1,3\text{-}C_4H_6$ at 1 atm. The net rate of formation of the adducts ($C_{10}H_{11}^{l}$, $C_{10}H_{11}^{c5}$, and $C_{10}H_{11}^{c6}$) was set equal to zero. Backward reaction refers to $C_{10}H_{11}^{l*} \rightarrow C_6H_5 + 1,3\text{-}C_4H_6$.

For instance, the rate of formation of $C_{10}H_{11}^{l*}$ increases by 1 order of magnitude with respect to the value that would be determined using vibrational partition functions. Analogously, the preexponential factor for the reaction of the formation of $C_{10}H_{11}^{c5*}$ decreases from 1.3×10^{11} to 3.1×10^{10}, and that of the reaction of formation of $C_{10}H_{11}^{c6*}$ decreases from 1.9×10^{11} to 4.6×10^{10}.

3.3. QRRK Calculation of Rate Parameters for $1,3\text{-}C_4H_6 + C_6H_5$. QRRK theory was used to estimate the overall reaction rate for the formation of the products of the reaction between $1,3\text{-}C_4H_6$ and C_6H_5. The mean vibrational frequencies for activated adducts $C_{10}H_{11}^{l*}$, $C_{10}H_{11}^{c5*}$, and $C_{10}H_{11}^{c6*}$ were determined, using vibrational frequencies evaluated with quantum chemistry, to be 977.2, 1107.4, and 1070.9 cm^{-1}, respectively. The QRRK rate coefficients for the reaction of the production of $C_{10}H_{10}^{l}$, $C_{10}H_{11}^{c6}$, and $C_9H_8^{c5}$, calculated at 1 atm as a function of temperature, are shown in Figure 8. The rate coefficient of the backward reaction from excited $C_{10}H_{11}^{l*}$ is also reported for comparison. As its rate increases, the rate of all of the other reactions correspondingly decreases. The species produced in the largest amount is $C_{10}H_{11}^{l}$, followed by $C_{10}H_{10}^{c6}$, $C_{10}H_{10}^{l}$, and $C_9H_8^{c5}$. The higher rate of production of $C_{10}H_{10}^{c6}$ with respect to that of $C_9H_8^{c5}$ is determined by a combined thermodynamic and kinetic effect: the formation of $C_{10}H_{11}^{c6*}$ is thermodynamically more stable by 15 kcal/mol than the formation of $C_{10}H_{11}^{c5*}$, whereas the activation energy for the formation of $C_{10}H_{11}^{c6*}$ is about 20 kcal/mol smaller than that for the formation of $C_{10}H_{11}^{c5*}$. Finally, the rate of production of $C_{10}H_{10}^{c6}$ is higher than that of $C_9H_8^{c5}$ because its rate of formation from $C_{10}H_{11}^{c6*}$ is faster than that for the formation of $C_9H_8^{c5}$ from $C_{10}H_{11}^{c5*}$.

The products formed through collisional stabilization, $C_{10}H_{11}^{l}$, $C_{10}H_{11}^{c5}$, and $C_{10}H_{11}^{c6}$, are thermodynamically unstable at high temperatures and are therefore likely to react rapidly. So in a situation where N_2 is the most abundant species, we can assume that, once generated, they get back to their excited states through collisional excitation and react through the mechanism reported in Figure 2. This assumption is reproduced, imposing a zero net production rate for these species. The results of the QRRK calculations performed under this hypothesis are shown in Figure 9. The species produced at the highest rate is now $C_{10}H_{10}^{c6}$ with an increase in the QRRK rate coefficient, with respect to the previous case, of 3 orders of magnitude at 1000 K. A similar effect is observed for the rate of formation of $C_9H_8^{c5}$. The kinetic parameters of the QRRK rates for the formation of all of the considered species were fit through nonlinear regression both for the case in which the formation of the stabilized adduct was neglected and for the case in which it was not. The results, interpolated at two different pressures (1 and 0.01 atm), are reported in Table 5.

It is now interesting to analyze the relative contributions of the different reaction channels considered in the overall kinetic scheme. If we consider the $C_{10}H_{11}$ adducts to be stable species, then at 1000 K and 1 atm the relative logarithmic rates of

TABLE 5: QRRK Rate Coefficients for the Reaction between C_6H_5 and 1,3-C_4H_6[a]

Products: $C_9H_8^{c5}$, $C_{10}H_{10}^{c6}$, $C_{10}H_{10}^{l}$

	$P = 1$ atm			$P = 0.01$ atm		
reaction	$\log_{10}A$	α	E_a	$\log_{10}A$	α	E_a
$C_6H_5 + 1,3\text{-}C_4H_6 \rightarrow C_9H_8^{c5} + CH_3$	13.2	−1.35	5167.	13.2	−1.35	5167.
$\rightarrow C_{10}H_{10}^{c6} + H$	23.7	−4.01	1178.	23.7	−4.01	1178.
$\rightarrow C_{10}H_{10}^{l} + H$	14.0	−1.00	6685.	14.0	−1.00	6685.

Products: $C_9H_8^{c5}$, $C_{10}H_{10}^{c6}$, $C_{10}H_{10}^{l}$, $C_{10}H_{11}^{c6}$, $C_{10}H_{11}^{c5}$

	$P = 1$ atm			$P = 0.01$ atm		
reaction	$\log_{10}A$	α	E_a	$\log_{10}A$	α	E_a
$C_6H_5 + 1,3\text{-}C_4H_6 \rightarrow C_9H_8^{c5} + CH_3$	33.0	−6.65	25 593.	22.1	−3.79	12 530.
$\rightarrow C_{10}H_{10}^{c6} + H$	40.3	−8.43	19 138.	32.0	−6.29	8400.
$\rightarrow C_{10}H_{10}^{l} + H$	22.3	−3.23	14 736.	18.9	−2.36	10 740.
$\rightarrow C_{10}H_{11}^{c5}$	50.8	−12.57	24 826.	39.1	−10.07	11 378.
$\rightarrow C_{10}H_{11}^{c6}$	63.3	−15.78	19 641.	56.1	−14.52	9870.

Products: $C_9H_8^{c5}$, $C_{10}H_{10}^{c6}$, $C_{10}H_{10}^{l}$, $C_{10}H_{11}^{c6}$, $C_{10}H_{11}^{c5}$, $C_{10}H_{11}^{l}$

	$P = 1$ atm			$P = 0.01$ atm		
reaction	$\log_{10}A$	α	E_a	$\log_{10}A$	α	E_a
$C_6H_5 + 1,3\text{-}C_4H_6 \rightarrow C_9H_8^{c5} + CH_3$	22.5	−3.33	30 556.	36.8	−7.71	28 365.
$\rightarrow C_{10}H_{10}^{c6} + H$	35.7	−6.79	29 018.	45.7	−9.89	25 181.
$\rightarrow C_{10}H_{10}^{l} + H$	20.4	−2.32	25 529.	34.9	−6.64	27 320.
$\rightarrow C_{10}H_{11}^{c6}$	43.1	−10.04	32 286.	52.1	−13.47	27 644.
$\rightarrow C_{10}H_{11}^{c5}$	52.8	−12.46	27 208.	65.0	−16.72	25 269.
$\rightarrow C_{10}H_{11}^{l}$	46.7	−10.2	16 508.	67.6	−16.85	23 305.

[a] Three cases involving different products were considered. The kinetic constant values were fitted between 500 and 2500 K at 1 and 0.01 atm. $k = A \cdot T^{\alpha} \cdot \exp(-E_a/RT)$. Preexponential factors and activation energies are reported in units consistent with cal, s, mol, and cm.

formation of $C_{10}H_{10}^{c6}$, $C_{10}H_{10}^{l}$, $C_{10}H_{11}^{l}$, $C_{10}H_{11}^{c5}$, and $C_{10}H_{11}^{c6}$ with respect to $C_9H_8^{c5}$ are 1.6, 1.33, 2.29, 1.01, and 1.72, respectively. If we neglect the formation of stabilized adducts, then the relative logarithmic rates of formation of $C_{10}H_{10}^{c6}$, $C_{10}H_{10}^{l}$, and $C_9H_8^{c5}$ under the same conditions become 1.57, 1.23, and 1, respectively. Finally, we can observe from Figure 9 that when the temperature increases the formation rate of $C_9H_8^{c5}$ increases correspondingly, whereas that of $C_{10}H_{10}^{c6}$ decreases, though the formation of $C_{10}H_{10}^{c6}$ is kinetically preferred over that of $C_9H_8^{c5}$ in the investigated range of temperatures.

On the whole, it is difficult to evaluate the impact that this reaction might have on the rate of formation of naphthalene in a flame without inserting it into a detailed kinetic mechanism and performing simulations. However, a direct comparison with two of the mechanisms most used to explain the formation of PAH in a flame, namely, the HACA mechanism[8] and the cyclopentadienyl pathway,[11] is possible under certain assumptions. In fact, a necessary step of the HACA mechanism is the addition of C_2H_2 to phenyl, whose rate is equal to 1.58×10^{11} $cm^3/(mol \cdot s)$ at 1000 K,[28] whereas according to the cyclopentadienyl pathway naphthalene is generated as a product of the reaction between two cyclopentadienyl radicals[10,29]

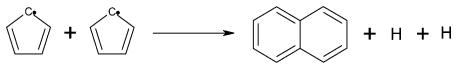

At 1000 K, the rate of this reaction is equal to 3.57×10^{11} $cm^3/(mol\ s)$.[11] Because the concentration of C_5H_5 is often of the same order of magnitude as that of C_6H_5,[30] the kinetic constants of the reaction of formation of naphthalene through the HACA and C_5H_5 mechanisms can be compared to the value here calculated (2.6×10^{11} $cm^3/(mol \cdot s)$ at 1000 K), remembering that the rate of the process is proportional to the product of the kinetic constant and the concentration of the reactants. Because in the framework of this work $C_{10}H_{10}^{c6}$ can be considered to be a precursor of naphthalene, it appears that the reaction pathway here proposed can account for the formation of naphthalene and higher PAH in a flame, provided that 1,3-C_4H_6 is present in a concentration comparable to that of C_2H_2 or C_5H_5, as is the case for butadiene flames.

Among the different mechanisms proposed for indene formation, the addition of allene (C_3H_4) to the phenyl radical[7] appears to be fast enough to explain the experimental results:

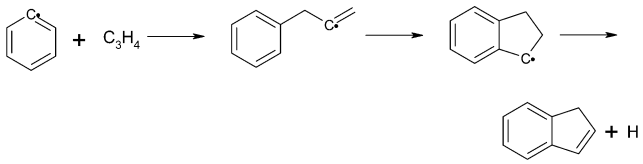

The first reaction of this mechanism is considered to be the rate-determining step of the process, with a kinetic constant value of 1×10^{13} $cm^3/(mol \cdot s)$ at 1000 K. Following the above-reported discussion on the formation of naphthalene, this value can be compared with 1.6×10^8 $cm^3/(mol \cdot s)$, which is the formation rate of indene that we calculated at 1000 K when the formation of stabilized adducts was neglected. Because it is unlikely that 1,3-C_4H_6 is present in a flame in a high enough concentration to compensate for a difference of 5 orders of magnitude between the two kinetic constants, we concluded that this reaction is not a viable route to the formation of indene.

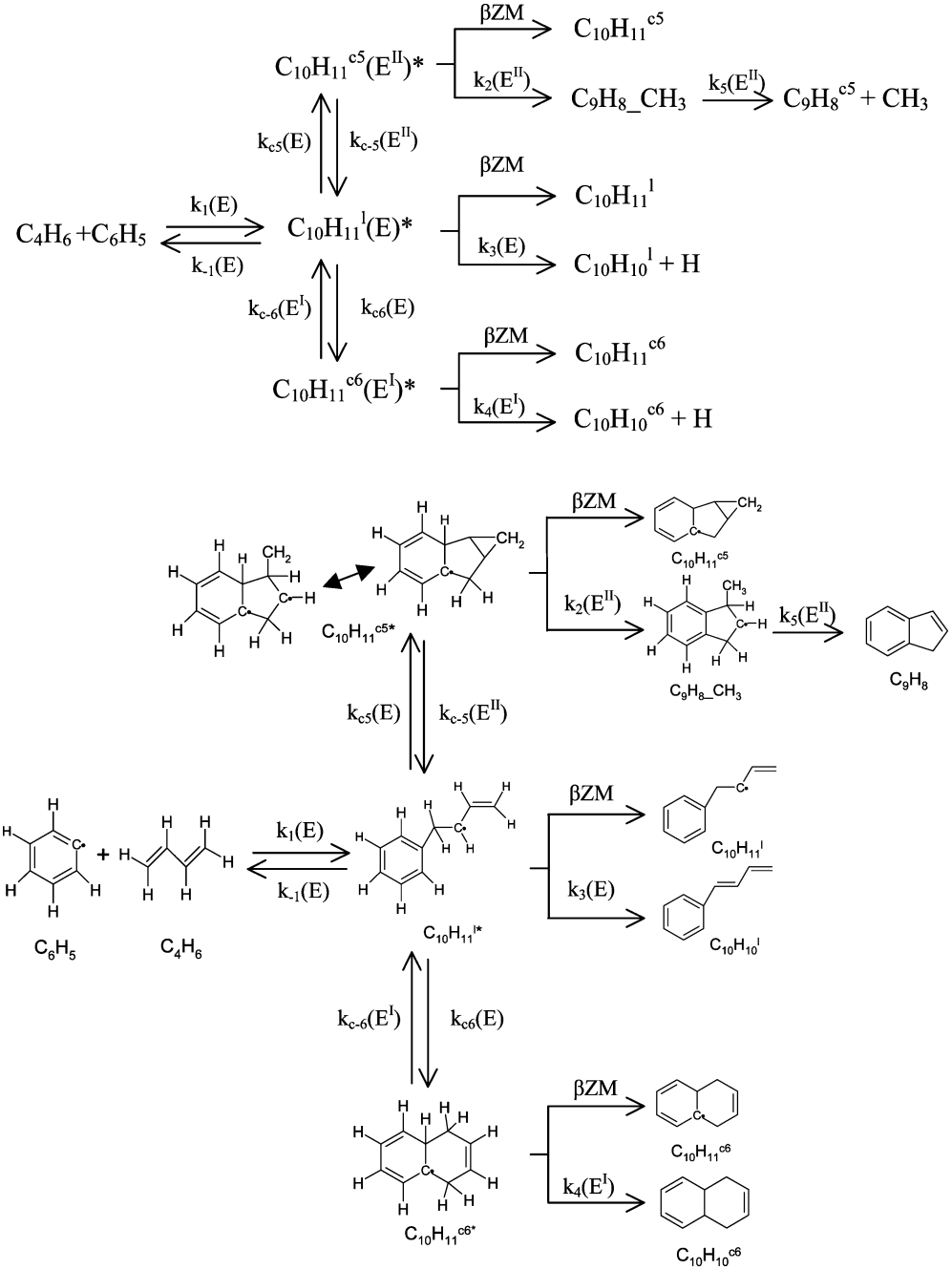

Figure 10. Kinetic pathway following the reaction of the addition of 1,3-butadien-1-yl to C_6H_6.

Finally, it is interesting to compare the QRRK rate of formation of 1,3-dihydronaphthalene with that of 1,3-exadiene from C_2H_3 and 1,3-C_4H_6 discussed in our previous work.[6] In the investigated range of temperature, the two logarithmic kinetic constants differ by a maximum factor of 1.08. This relatively small difference suggests that 1,3-butadiene, when reacting with an alkene radical such as C_2H_3 or C_6H_5, can easily give cyclization reactions regardless of the dimensionality of the reacting alkene, thus contributing significantly to the formation of PAH when a large amount of 1,3-C_4H_6 is available. However, the formation rate of $C_9H_8^{c5}$, which can be considered in the framework of this work to be a precursor to indene, is much smaller than that for cyclopentadiene.[6] This means that whereas reaction pathways involving 1,3-C_4H_6 can contribute significantly to the formation of the first five-membered aromatic ring the reaction of 1,3-C_4H_6 with the phenyl radical is not likely to be a viable pathway to the formation of indene.

3.4. Kinetics of the 1,3-Butadien-1-yl + C_6H_6 Reaction. Experimental data show that the 1,3-butadien-1-yl radical can be easily formed in butadiene flames.[31] Therefore, to investigate its possible contribution to the formation of naphthalene, we investigated the reaction between 1,3-butadien-1-yl and C_6H_6 to form the $C_{10}H_{11}^{l*}$ adduct by hydrogen transposition. This second kinetic scheme is summarized in Figure 10. In the first reaction, 1,3-butadien-1-yl binds to C_6H_6 to form the $C_4H_5\_C_6H_6$* adduct, which successively reacts to give the $C_{10}H_{11}^{l*}$ adduct through the transposition of a hydrogen atom from the C6 ring to the butadienic tail. Activation energies and reaction enthalpy changes for the first two reactions were evaluated at the G2MP2* level and are reported in Figure 11, and transition states are shown in Figure 12. Enthalpy changes calculated at different levels of theory for the two investigated reactions are reported in Table 6, where once again it can be observed that G2MP2* and DFT predictions differ significantly.

TABLE 6: Comparison of Reaction Enthalpy Changes (kcal/mol) Calculated at 298 K and 1 atm with Different Quantum Chemistry Theories[a]

	B3LYP 6-31g(d,p)	QCISD(T) 6-311+g(d,p)	MP2 6-311+g(3df,2p)	MP2 6-311+g(d,p)	G2MP2*
1,3-C_4H_5 + C_6H_6 → C_4H_5_C_6H_6	−20.7	−26.9	−25.0	−24.6	−25.5
C_4H_5_C_6H_6 → $C_{10}H_{11}^{l}$	−25.3	−23.0	−36.6	−36.2	−22.9

[a] G2MP2* is different from the original G2MP2 method in that geometries were optimized with B3LYP/6-31g(d,p). All energies are corrected for ZPE and thermal energies with frequencies calculated with B3LYP/6-31g(d,p)

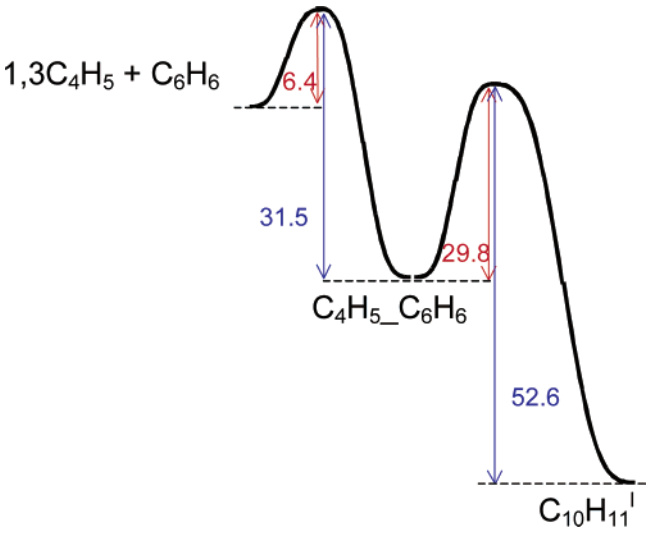

Figure 11. Enthalpy changes and activation energies for the reaction between 1,3-butadien-1-yl and benzene (kcal/mol). All values were calculated with the G2MP2* theory.

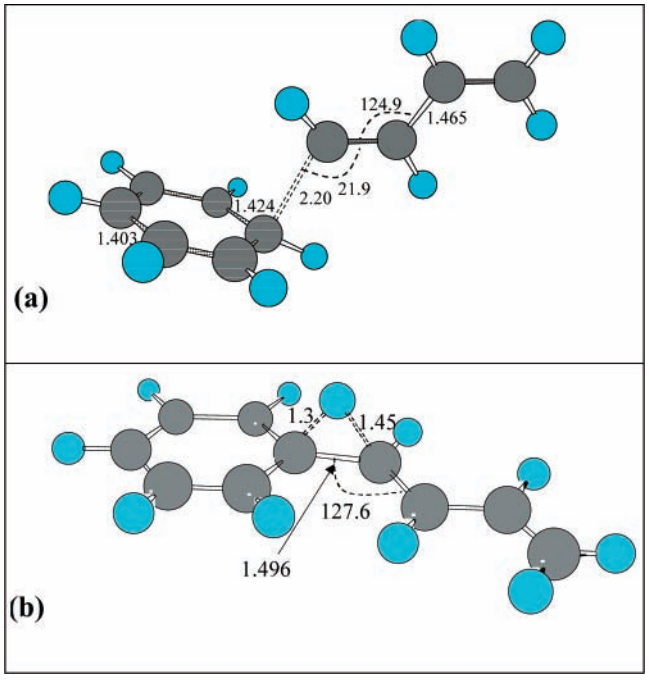

Figure 12. Transition-state structures for reactions (a) 1,3-C_4H_5 + C_6H_6 → C_4H_5_C_6H_6 and (b) C_4H_5_C_6H_6 → $C_{10}H_{11}^{l}$. Distances are reported in angstroms, and angles are reported in degrees.

Also, in this case, the vibrational analysis revealed the presence of some low vibrational frequencies. In particular, the transition state of the first reaction presents one low vibrational frequency (21.13 cm^{-1}) whose value is similar to 22.4 cm^{-1} previously found for the transition state of the reaction between 1,3-C_4H_6 and C_6H_5 and corresponds to the torsional motion around the butadiene−benzene bond. Consequently, as previously discussed, its partition function was evaluated with eqs 7 and 10 using the calculated rotational potential energy. The energetic barrier corresponding to this internal rotation is low (about 1.1 kcal/mol), and the associated rotational partition function is 19.37. On the contrary, the second transition state presents some low vibrational frequencies, but because of the geometric configuration of the TST, the corresponding rotational motions are blocked by significant energy barriers. The C_4H_5_C_6H_6* adduct has a small vibrational frequency of 40.01 cm^{-1}, which corresponds to the relative motion of C_6H_6 and C_4H_5 around the butadiene−benzene bond. Its rotational potential energy is higher than the corresponding value in $C_{10}H_{11}^{l}$ (3.3 vs 1.9 kcal/mol). As a result of the relatively high rotational activation energy, the difference between vibrational and rotational partition functions (5.25 vs 5.44) is small, which means that this frequency can be treated as a vibration without committing any significant error. The calculated vibrational and internal rotation partition functions for the reactant and transition state are reported in Table 7.

TABLE 7: Comparison between Vibrational (Q_{vib}) and Internal Rotational (Hindered and Free) Partition Functions for Significant Low Vibrational Frequencies[a]

	ν [cm^{-1}]	Q_{vib}	Q_{rot}^{hind}	Q_{rot}^{free}
TST1 internal rotor	21.13	10.37	19.37	37.87
C_4H_5_C_6H_6 butadiene rotation	44.01	5.25	5.44	39.74

[a] TST1 is the transition state for the 1,3-C_4H_5 + C_6H_6 → C_4H_5_C_6H_6 reaction.

3.5. QRRK Calculation of Rate Parameters for the 1,3-Butadien-1-yl + C_6H_6 Reaction. QRRK theory was used to calculate the rate parameters for the reaction of 1,3-butadien-1-yl with C_6H_6, which was similar to what was done previously. In this case, the mechanism leading to the formation of the $C_{10}H_{11}^{l*}$ excited complex requires two successive reactions. The first is the formation of the C_4H_5_C_6H_6* excited complex, which can then dissociate into the reactants or proceed to form $C_{10}H_{11}^{l*}$ by the transposition of a hydrogen atom. The calculated kinetic parameters for these two reactions are reported in Table 8. Because the energy barrier to form $C_{10}H_{11}^{l*}$ (29.8 kcal/mol) is smaller than that for the dissociation to C_4H_5_C_6H_6* (52.6 kcal/mol), it follows that the k_S kinetic constant is always considerably larger than the corresponding k_{-S} backward reaction so that the mechanism of the two first reactions can be summarized as

$$1,3\text{-}C_4H_5 + C_6H_6 \underset{k_{-F}}{\overset{k_F}{\rightleftarrows}} C_4H_5\_C_6H_6^{*} \qquad (11)$$

$$C_4H_5\_C_6H_6^{*} \xrightarrow{k_S} C_{10}H_{11}^{l*} \qquad (12)$$

Because C_4H_5_C_6H_6* is a very reactive species, the pseudo-steady-state approximation can be applied to determine its concentration as a function of the concentrations of 1,3-butadien-1-yl and C_6H_6 and of the kinetic constants k_F, k_{-F}, and k_S.

TABLE 8: Calculated TST Kinetic Constants ($k = A \cdot T^{\alpha} \cdot \exp(-E/RT)$)[a]

	reaction	A_{forw}	α	$E_{a,forw}$	A_{back}	α	$E_{a,back}$
k_F	1,3-$C_4H_5 + C_6H_6 \rightarrow C_4H_5\_C_6H_6$	1.3×10^{11}	0.	6.4	1.8×10^{16}	−1.	31.5
k_S	$C_4H_5\_C_6H_6 \rightarrow C_{10}H_{11}^{l}$	1.6×10^{12}	0.	29.8	1.1×10^{12}	0.	52.6

[a] Kinetic parameters are reported in units consistent with kcal, s, mol, and cm and were modified treating low vibrational frequencies as internal rotors, when necessary. The rate coefficients of the backward reactions were calculated through thermodynamic consistency with calculated free-energy changes.

TABLE 9: QRRK Rate Coefficients for the Reaction of 1,3-Butadien-1-yl with C_6H_6[a]

Products: $C_9H_8^{c5}$, $C_{10}H_{10}^{c6}$, $C_{10}H_{10}^{l}$

	$P = 1$ atm			$P = 0.01$ atm		
reaction	$\log_{10}A$	α	E_a	$\log_{10}A$	α	E_a
1,3-$C_4H_5 + C_6H_6 \rightarrow C_9H_8^{c5} + CH_3$	7.5	0.63	44 607.	7.5	0.63	44 607.
$\rightarrow C_{10}H_{10}^{c6} + H$	7.8	0.71	31 255.	7.8	0.71	31 255.
$\rightarrow C_{10}H_{10}^{l} + H$	8.3	0.98	46 496.	8.3	0.98	46 496.

Products: $C_9H_8^{c5}$, $C_{10}H_{10}^{c6}$, $C_{10}H_{10}^{l}$, $C_{10}H_{11}^{c6}$, $C_{10}H_{11}^{c5}$

	$P = 1$ atm			$P = 0.01$ atm		
reaction	$\log_{10}A$	α	E_a	$\log_{10}A$	α	E_a
1,3-$C_4H_5 + C_6H_6 \rightarrow C_9H_8^{c5} + CH_3$	28.0	−4.92	64 508.	13.1	−0.92	49 087.
$\rightarrow C_{10}H_{10}^{c6} + H$	25.0	−3.90	48 629.	15.0	−1.29	36 477.
$\rightarrow C_{10}H_{10}^{l} + H$	8.3	0.98	46 496.	8.3	0.98	46 496.
$\rightarrow C_{10}H_{11}^{c6}$	35.4	−7.86	35 681.	41.0	−10.2	33 559.
$\rightarrow C_{10}H_{11}^{c5}$	4.4	−10.36	60 461.	21.8	−5.01	38 882.

Products: $C_9H_8^{c5}$, $C_{10}H_{10}^{c6}$, $C_{10}H_{10}^{l}$, $C_{10}H_{11}^{c6}$, $C_{10}H_{11}^{c5}$, $C_{10}H_{11}^{l}$

	$P = 1$ atm			$P = 0.01$ atm		
reaction	$\log_{10}A$	α	E_a	$\log_{10}A$	α	E_a
1,3-$C_4H_5 + C_6H_6 \rightarrow C_9H_8^{c5} + CH_3$	28.4	−5.03	64 993.	13.1	−0.92	49 086.
$\rightarrow C_{10}H_{10}^{c6} + H$	26.0	−4.18	49 558.	15.1	−1.31	36 523.
$\rightarrow C_{10}H_{10}^{l} + H$	9.0	−0.80	47 171.	8.3	0.97	46 519.
$\rightarrow C_{10}H_{11}^{c6}$	37.3	−8.40	37 425.	41.0	−10.2	33 575.
$\rightarrow C_{10}H_{11}^{c5}$	44.5	−10.52	61 069.	21.8	−5.01	38 886.
$\rightarrow C_{10}H_{11}^{l}$	16.3	−2.39	5048.	8.7	−0.86	−45.9

[a] Three cases involving different products were considered. The kinetic constant values were fit between 500 and 2500 K at 1 and 0.01 atm. $k = A \cdot T^{\alpha} \cdot \exp(-E_a/RT)$. Preexponential factors and activation energies are reported in units consistent with cal, s, mol, and cm.

Accordingly, the rate of formation of $C_{10}H_{11}^{l}$ can be described by the global reaction

$$1,3\text{-}C_4H_5 + C_6H_6 \underset{k_{back}}{\overset{k_{forw}}{\leftrightarrow}} C_{10}H_{11}^{l*} \qquad (13)$$

whose forward rate is equal to

$$R = k_S[C_4H_5\_C_6H_6^{*}] = \frac{k_F \cdot k_S}{k_{-F} + k_S}[1,3\text{-}C_4H_5][C_6H_6] = k_{forw}[1,3\text{-}C_4H_5][C_6H_6] \qquad (14)$$

Because in the 500−2500 K temperature range the value of k_S is significantly smaller than the value of k_{-F} the kinetic constant k_{forw} can be approximated as

$$k_{forw} \approx \frac{k_F \cdot k_S}{k_{-F}} \qquad (15)$$

The kinetic constant of the reaction giving back the 1,3-butadien-1-yl and C_6H_6 reactants from $C_{10}H_{11}^{l*}$ (k_{back}) was calculated from k_{forw} by imposing thermodynamic consistency. The values of the kinetic parameters so calculated are $k_{forw} = 1.2 \times 10^{7} \cdot T \cdot \exp(-4.7/RT)$ and $k_{back} = 2.2 \times 10^{12} \cdot \exp(-53.1/RT)$. In this case, the activation energy of the reaction involving 1,3-butadien-1-yl is larger than that involving C_6H_6 (53.1 vs 48.9). This means that the backward reaction from $C_{10}H_{11}^{l*}$ to the reactants is globally slower for the 1,3-butadien-1-yl + C_6H_6 mechanism than for the 1,3-C_4H_6 + C_6H_5 one.

The QRRK rate constants for the reactions of the production of $C_{10}H_{10}^{l}$, $C_{10}H_{10}^{c6}$, and $C_9H_8^{c5}$ calculated at 1 atm as a function of temperature are reported in Figure 13. The QRRK rate coefficient for the backward reaction from excited $C_{10}H_{11}^{l*}$ is also reported for comparison. Different from what observed for the 1,3-C_4H_6 + C_6H_5 reaction, the rate of the global reaction is almost insensitive to the value of the backward reaction. The species produced in the largest amount is always $C_{10}H_{10}^{c6}$, followed by $C_{10}H_{10}^{l}$ and $C_9H_8^{c5}$. However, even if the trend of the products is not changed with respect to that reported in Figure 8, the absolute values are smaller. Particularly, the rate of formation of $C_{10}H_{10}^{l}$ adducts at 1000 K and 1 atm decreases by 2.6 orders of magnitude. This dramatic decrease in the overall rate constants is determined by the decrease in the rate of formation of the $C_{10}H_{11}^{l*}$ adduct, which in turn determines a decrease in the rate of formation of all of the products of the

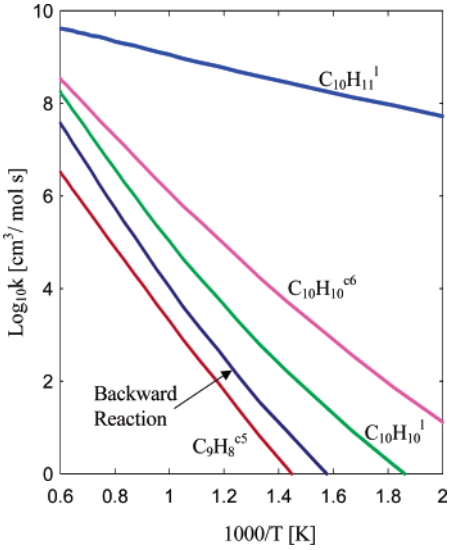

Figure 13. QRRK rate constants calculated for the reaction of 1,3-butadien-1-yl with benzene at 1 atm. All possible products were considered. Backward reaction refers to $C_{10}H_{11}^{l*} \rightarrow$ 1,3-C_4H_5 + C_6H_6.

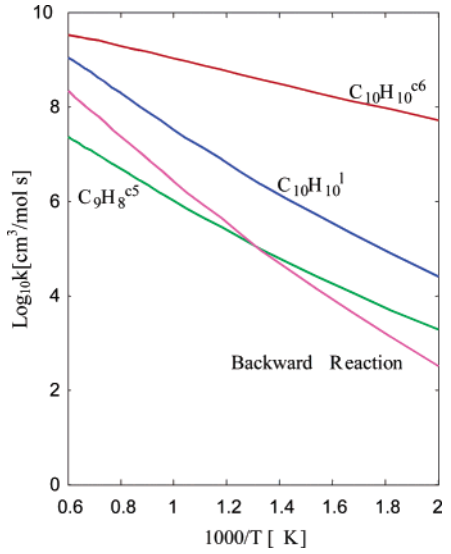

Figure 14. QRRK rate constants calculated for the addition of 1,3-butadien-1-yl to C_6H_6 at 1 atm. The net rate of formation of adducts ($C_{10}H_{11,}^{l}$ $C_{10}H_{11}^{c5}$, and $C_{10}H_{11}^{c6}$) was set equal to zero. Backward reaction refers to $C_{10}H_{11}^{l*} \rightarrow$ 1,3-C_4H_5 + C_6H_6.

reaction. Also, in this case, to account for the thermodynamic instability of $C_{10}H_{11}^{l}$, $C_{10}H_{11}^{c5}$, and $C_{10}H_{11}^{c6}$, the net production rate of these species was assumed to be equal to zero, thus imposing that they can give back only the excited species. The QRRK rate constants so calculated are shown in Figure 14. The species produced at the highest rate is always $C_{10}H_{10}^{c6}$, whose QRRK rate coefficient, with respect to the case in which the formation of all of the species was considered, increases by 3 orders of magnitude at 1000 K. This situation is similar to that found for the butadiene−phenyl case. The same trend is observed for the formation rate of $C_9H_8^{c5}$.

As previously done, the kinetic constant parameters for the formation of all species were fit through nonlinear regression, and the results are reported in Table 9 for two different pressures,1 and 0.01 atm.

Summary and Conclusions

Reactions mechanisms involving C4 species and resonantly stabilized radicals can be important in various combustion environments. In this work, we investigated, using quantum chemistry and QRRK theory, the leading kinetic pathways from 1,3-C_4H_6 + C_6H_5 and 1,3-C_4H_5 + C_6H_6 to naphthalene. It was found that, at least in combustion environments where a significant amount of the C4 species is present, reactions leading to naphthalene and indene cannot be disregarded with respect to other mechanisms proposed in the literature. However, the reaction channel involving 1,3-butadien-1-yl has been found to be kinetically unfavorable with respect to that involving 1,3-C_4H_6. Consequently, it can play a role only when the relative concentration of the C4 species overcomes the kinetic constraint. We also found that the production of indene through the reaction pathways here investigated requires overcoming a significant activation energy, which suggests that indene is formed in flames through alternative reaction channels.

The kinetic constants of reactions leading to naphthalene through the 1,3-C_4H_6 + C_6H_5 pathway are almost the same as those leading to benzene from 1,3-C_4H_6 + C_2H_3 in a wide temperature range. This seems to indicate that the rate of 1,3-C_4H_6 addition to C_2H_3 or C_6H_5, if it results in the formation of a resonantly stabilized radical, is the same regardless of the molecular structure of the reactant. However, the kinetic constants of reactions leading to five-membered ring species are quite different. In particular, whereas the reaction leading to a single five-membered ring is even faster than that leading to a single six-membered ring, the opposite is true for species involving two rings. In the latter case, the formation of indene is by far much slower than that of $C_{10}H_{11}^{C6}$, which can be regarded in this context as a naphthalene precursor.

Finally, it was found that errors as large as 1 order of magnitude on calculated kinetic constants can arise when calculating partition functions of internal motions either as free internal rotations or as vibrations rather then as partially hindered internal rotations.

Acknowledgment. We are indebted to Professors E. Ranzi and T. Faravelli for continuous and fruitful discussions.

References and Notes

(1) Kunzli, N.; Kaiser, R.; Medina, S.; Studnicka, M.; Chanel, O.; Filliger, P.; Herry, M.; Horak, F.; Puybonnieux-Texier, V.; Quenel, P.; Schneider, J.; Seethaler, R.; Vergnaud, J. C.; Sommer, H. *Lancet* **2000**, *356*, 795.

(2) Durant, J. L.; Busby, W. F.; Lafleur, A. L.; Penman, B. W.; Crespi, C. L. *Mutat. Res.-Genet. Toxicol.* **1996**, *371*, 123.

(3) Siegmann, K.; Siegmann, H. C. Molecular Precursor of Soot and Quantification of the Associated Health Risk. In *Current Problems in Condensed Matter*. Morán-Lopez, J. L., Ed.; Plenum Press: New York, 1998.

(4) Richter, H.; Howard, J. B. *Prog. Energy Combust. Sci.* **2000**, *26*, 565.

(5) Violi, A.; D'Anna, A.; D'Alessio, A. *Chem. Eng. Sci.* **1999**, *54*, 3433.

(6) Cavallotti, C.; Rota, R.; Carra, S. *J. Phys. Chem. A* **2002**, *106*, 7769.

(7) Lindstedt, P.; Maurice, L.; Meyer, M. *Faraday Discuss.* **2001**, *119*, 409.

(8) Frenklach, M.; Warnatz, J. *Combust. Sci. Technol.* **1987**, *51*, 265.

(9) Appel, J.; Bockhorn, H.; Frenklach, M. *Combust. Flame* **2000**, *121*, 122.

(10) Marinov, N. M.; Pitz, W. J.; Westbrook, C. K.; Castaldi, M. J.; Senkan, S. M. *Combust. Sci. Technol.* **1996**, *116*, 211.

(11) Marinov, N. M.; Pitz, W. J.; Westbrook, C. K.; Vincitore, A. M.; Castaldi, M. J.; Senkan, S. M.; Melius, C. F. *Combust. Flame* **1998**, *114*, 192.

(12) Alkemade, U.; Homann, K. H. *Z. Phys. Chem.* **1989**, *161*, 19.

(13) Goldaniga, A.; Faravelli, T.; Ranzi, E. *Combust. Flame* **2000**, *122*, 350.

(14) Dean, A. M. *J. Phys. Chem.* **1985**, *89*, 4600.

(15) Troe, J. *J. Chem. Phys.* **1977**, *66*, 4745.

(16) Frisch, M. J.; Trucks, G. W.; Schlegel, H. B.; Scuseria, G. E.; Robb, M. A.; Cheeseman, J. R.; Zakrzewski, V. G.; Montgomery, J. A., Jr.; Stratmann, R. E.; Burant, J. C.; Dapprich, S.; Millam, J. M.; Daniels, A. D.; Kudin, K. N.; Strain, M. C.; Farkas, O.; Tomasi, J.; Barone, V.; Cossi, M.; Cammi, R.; Mennucci, B.; Pomelli, C.; Adamo, C.; Clifford, S.; Ochterski, J.; Petersson, G. A.; Ayala, P. Y.; Cui, Q.; Morokuma, K.; Malick, D. K.; Rabuck, A. D.; Raghavachari, K.; Foresman, J. B.; Cioslowski, J.; Ortiz, J. V.; Stefanov, B. B.; Liu, G.; Liashenko, A.; Piskorz, P.; Komaromi, I.; Gomperts, R.; Martin, R. L.; Fox, D. J.; Keith, T.; Al-Laham, M. A.; Peng, C. Y.; Nanayakkara, A.; Gonzalez, C.; Challacombe, M.; Gill, P. M. W.; Johnson, B. G.; Chen, W.; Wong, M. W.; Andres, J. L.; Head-Gordon, M.; Replogle, E. S.; Pople, J. A. *Gaussian 98*, revision A.6; Gaussian, Inc.: Pittsburgh, PA, 1998.

(17) Lee, C. Y., W.; Parr, R. G. *Phys. Rev. B* **1988**, *37*, 785.

(18) Curtiss, L. A.; Raghavachari, K.; Pople, J. A. *J. Chem. Phys.* **1995**, *103*, 4192.

(19) Raghavachari, K.; Anderson, J. B. *J. Phys. Chem.* **1996**, *100*, 12960.

(20) Truhlar, D. G.; Garrett, B. C.; Klippenstein, S. J. *J. Phys. Chem.* **1996**, *100*, 12771.

(21) Hirschfelder, J. O.; Wigner, E. *J. Chem. Phys.* **1939**, *7*, 616.

(22) Van Speybroeck, V.; Van Neck, D.; Waroquier, M.; Wauters, S.; Saeys, M.; Marin, G. B. *J. Phys. Chem. A* **2000**, *104*, 10939.

(23) Pitzer, K. S.; Gwinn, W. D. *J. Chem. Phys.* **1942**, *10*, 428.

(24) Gilbert, R. G.; Smith, S. C. *Theory of Unimolecular and Recombination Reactions*; Blackwell Scientific Publications: Oxford, England, 1990.

(25) Oxgaard, J.; Wiest, O. *J. Phys. Chem. A* **2001**, *105*, 8236.

(26) Oxgaard, J.; Wiest, O. *J. Phys. Chem. A* **2002**, *106*, 3967.

(27) Carrà, S.; Raimondi, M.; Simonetta, M. *Tetrahedron* **1966**, *22*, 2673.

(28) Wang, H.; Frenklach, M. *Combust. Flame* **1997**, *110*, 173.

(29) Castaldi, M. J.; Marinov, N. M.; Melius, C. F.; Huang, J.; Senkan, S. M.; Pitz, W. J.; Westbrook, C. K.; Twenty-sixth Symposium (International) on Combustion, Pittsburgh, PA, 1996.

(30) Richter, H.; Howard, J. B. *Phys. Chem. Chem. Phys.* **2002**, *4*, 2038.

(31) McEnally, C. S.; Pfefferle, L. D. *Combust. Flame* **1998**, *115*, 81.

(32) Bockhorn, H. *Soot Formation in Combustion: Mechanisms and Models*; Springer: Berlin, 1994.